Received: 11 April 2023 | *Revised:* 13 May 2023 | *Accepted:* 13 May 2023
DOI: 10.37917/ijeee.19.2.20 *Vol. 19 | Issue 2 | December 2023*

Iraqi Journal for Electrical and Electronic Engineering
Original Article

Open Access
IJEEE University of Basrah College of Engineering

Tri-Band Rectangular Microstrip Patch Antenna with Enhanced Performance for 5G Applications Using a π-Shaped Slot: Design and Simulation

AbdulGuddoos S. A. Gaid*, Mohammed A. M. Ali
Dept. of Communication & Computer Engineering, Faculty of Engineering and Information Technology, Taiz University, Taiz, Yemen

Correspondance
*AbdulGuddoos S. A. Gaid
Dept. of Communication & Computer Engineering,
Faculty of Engineering and Information Technology,
Taiz University, Taiz, Yemen
Email: quddoos.gaid@taiz.edu.ye

Abstract
In this study, we propose a compact, tri-band microstrip patch antenna for 5G applications, operating at 28 GHz, 38 GHz, and 60 GHz frequency bands. Starting with a basic rectangular microstrip patch, modifications were made to achieve resonance in the target frequency bands and improve S_{11} performance, gain, and impedance bandwidth. An inset feed was employed to enhance antenna matching, and a π–shaped slot was incorporated into the radiating patch for better antenna characteristics. The design utilized a Rogers RT/Duroid-5880 substrate with a 0.508 mm thickness, a 2.2 dielectric constant, and a 0.0009 loss tangent. The final dimensions of the antenna are 8 x 8.5 x 0.508 mm^3. The maximum S_{11} values obtained at the resonant frequencies of 27.9 GHz, 38.4 GHz, and 56 GHz are -15.4 dB, -18 dB, and -26.4 dB, respectively. The impedance bandwidths around these frequencies were 1.26 GHz (27.245 - 28.505), 1.08 GHz (37.775 - 38.855), and 12.015 GHz (51.725 - 63.74), respectively. The antenna gains at the resonant frequencies are 7.96 dBi, 6.82 dBi, and 7.93 dBi, respectively. Radiation efficiencies of 88%, 84%, and 90% were achieved at the resonant frequencies. However, it is observed that the radiation is maximum in the broadside direction at 28 GHz, although it peaks at $-41^o/41^o$ and $-30^o/30^o$ at 38 GHz and 56 GHz, respectively. Furthermore, the antenna design, simulations, and optimizations were carried out using HFSS, and the results were verified with CST. Both simulators showed a reasonable degree of consistency, confirming the effectiveness and reliability of the proposed antenna design.

Keywords
Rectangular microstrip patch antenna, Tri-band antenna, π-shaped slot, 5G applications, 28 GHz, 38 GHz, 60 GHz, HFSS, CST.

I. Introduction

Wireless communication technology has rapidly evolved to offer more efficient and less complex approaches for enhancing data transfer rates and providing high-quality services to customers. With the growing number of users connected to various wireless networks, future wireless systems must be able to manage this increasing demand [1]. Therefore, 5G technology has garnered attention due to its ability to transmit vast amounts of data at high speeds while reducing latency throughout the communication system [2] [3] [4] [5]. Developed countries have established 5G networks to meet these expectations. However, the current frequency spectra are becoming increasingly congested, leaving no bands available for future applications requiring wide frequency ranges. To overcome this challenge, researchers recommend switching to new frequency spectra that can provide the bandwidth required for conveying the massive amount of information created by the growing number of users [5] [6] [7] [8] [9] [10] [11] [12].

Therefore, the mm-wave spectrum, with higher data rates, wider bandwidths, and faster response times, is seen as the appropriate answer to these growing challenges. The mm-wave spectrum has a frequency range of 30 GHz to 300 GHz. Utilizing mm-wave frequencies in 5G networks has several advantages, including the availability of bands at 28 GHz, 38 GHz, and the unlicensed band at 60 GHz. Due to significant loss in free space path loss, penetration, and absorption losses in mm-wave communications, the same frequency can be reused repeatedly in a limited region with acceptable bandwidth efficiency. Furthermore, mm-wave communication is naturally safe and private due to its limited transmission range and narrow bandwidth. Sophisticated antenna arrays can also be developed and incorporated into printed circuit boards due to the small physical size of mm-wave antennas [13] [14] [15].

Antennas are essential components of wireless communication systems, and they must be designed to fit within the confines of small mobile devices. 5G antennas must also have a wide bandwidth and operate in multiple frequency bands. Additionally, mm-wave antennas must be energy-efficient, have high gain and directivity, and mitigate the effects of signal path loss and power requirements. To meet these demands, the Microstrip Patch Antenna (MSPA) technology is the best solution for 5G wireless networks [16] [17].

MSPAs are tiny, lightweight, inexpensive to produce, and easy to fabricate. They are also physically strong and can be mounted on virtually any surface, making them a suitable candidate for use in compact wireless devices and high-directional antenna arrays for base stations. However, MSPAs have some limitations due to substrate losses, copper losses, and surface waves, such as limited bandwidth, poor gain, and low efficiency [18] [19]. Therefore, several approaches are available to enhance MSPA performance, including feeding techniques, defective ground structure (DGS), etching slots and slits in the ground and on radiating elements, inserting metamaterial into the antenna's patch and ground plane, modifying the form of the patch, partial ground approaches, and multi-layer insulating substrates [20] [21] [22].

Several studies have been conducted on single, dual, or multi-band mm-wave frequencies, as documented in [23] [24] [25] [26] [27] [28] [29] [30] [31] [32]. The study presented in [23] introduced a small dual-band dolly-shaped antenna (DBDSA) that resonates at 23.52 GHz and 28.39 GHz. The antenna utilized a $7 \times 7 \times 1.28$ mm^3 Rogers RO3010 substrate with a dielectric constant of 10.2 and a loss tangent of approximately 0.0022. The DBDSA achieved an overall radiation efficiency of 80%, with a consistent gain of 5.51 dBi in the first band and a gain of 4.55 dBi in the second band. The lower band impedance bandwidth was 1.16 GHz (23.16 GHz - 24.32 GHz), while the upper band impedance bandwidth was 634 MHz (28.078 GHz - 28.712 GHz). However, the design has a complex geometrical structure, modest gain, and bandwidth.

Similarly, for future 5G communication systems, the work reported in [24] proposed a substrate-integrated waveguide (SIW) slot antenna. The antenna used a Rogers RT-duroid 5880 substrate with a height of 0.254 mm, a dielectric constant of 2.2, and a loss tangent of 0.003, with dimensions of $7.5 \times 27.06 \times 0.254$ mm^3. The suggested geometry consisted of a central circular ring and horizontal and vertical vias. The designed antenna resonated at 28.13 GHz and 37.97 GHz, with impedance bandwidths of 231 MHz and 92 MHz, respectively. The peak gains achieved in the lower and higher bands were 7.27 dBi and 8.46 dBi, respectively, with radiation efficiency of 88.25% and 86.30% in the lower and upper bands, respectively. However, this antenna had a large size and narrow bandwidth.

In [25], a compact, single-band, bow-tie-shaped microstrip patch antenna for wideband applications was described. The modified bow-tie structure was designed on top of an $8 \times 8 \times 0.787$ mm^3 Rogers RT-5880 dielectric substrate with $\varepsilon r = 2.2$ and $tan\delta = 0.0009$, supported by a full 0.017 mm thick copper ground. Diagonal slots inside the geometry were provided for exact resonance. The antenna had a return loss of 25.45 dB, a simulated impedance bandwidth of 1.88 GHz (26.81-28.69 GHz), a gain of 7.0 dBi, and a radiation efficiency of 74% at the resonance frequency of 27.77 GHz. Although this antenna had a small size, acceptable bandwidth, and good gain, its radiation efficiency was low, and it lacked multiband capabilities.

Masood Ur-Rehman et al. [26] proposed a tri-band slotted patch antenna operating at mm-wave frequencies of 28 GHz, 38 GHz, and 61 GHz. The suggested antenna had an overall dimension of $5.1 \times 5 \times 0.254$ mm^3 and was supplied by a microstrip line. The antenna was built on a single layer of Rogers RT/ Duroid 5880 printed circuit board with a thickness of 0.254 mm, a tangent loss of 0.0009, and a relative permittivity of 2.2. Three L- and F-shaped slots were put into the radiating patch. The antenna achieved peak gains of 7.2, 7.22, and 6.5 dBi in the three bands, with radiation efficiencies of 86%, 91%, and 85%, respectively. The -10 dB impedance bandwidths obtained at return losses of roughly 12, 22, and 12 dB were 0.84, 0.37, and 0.9 GHz, respectively. Despite its tiny size, adequate radiation efficiency, and reasonable gains, the return losses and realized bandwidths at the three bands were poor.

Fadwa Alnemr et al. [27] developed a dual-band circularly polarized antenna that operates at 28/38 GHz operating frequencies. The antenna was printed on a Rogers RT 5880 substrate with dimensions of 20.4×26.4 mm^2 and a thickness of 0.508 mm, with a circular hole in the patch's center and four slits in the corners. Microscopic holes on the patch's

edges were also carved to achieve the resonance frequencies and increase the return loss value. The single feed antenna exhibited return losses of 30 dB and 42 dB at 28/38 GHz, respectively. The single-element design could operate at frequencies ranging from 27.6 to 28.3 GHz in the 28 GHz band and from 35.2 to 47.2 GHz in the 38 GHz band.

In [18], a single-band antenna operating at 60 GHz was proposed. The antenna features a Q slot engraved on the radiating patch and is built on a 1.6 mm thick FR-4 substrate with a permittivity of 4.3. The overall dimensions of the antenna are $12.9 \times 14 \times 1.6$ mm^3, and it has a partial ground plane length of 2.2 mm. The antenna exhibits a resonance frequency of 60.06 GHz, an impedance bandwidth of 12.11 GHz, a return loss of 24 dB, a gain of 8.62, and a radiation efficiency of 82.15%. Despite its robust radiation characteristics, this antenna is a large single-band antenna.

In [29], a dual-band rectangular patch antenna was developed with two symmetric back-to-back L-shaped slots and a single square slot in the center. The antenna is constructed on a Rogers RT5880 substrate measuring $20 \times 16.5 \times 0.508$ mm^3, with a dielectric permittivity of 2.2 and a loss tangent of 0.0009. This antenna resonates at 25.98 GHz and 28.2 GHz, with return losses of 24.14 dB and 25.45 dB, and impedance bandwidths of 0.55 GHz and 1.1 GHz. The antenna achieves gains of 8.63 dBi and 11.26 dBi in both bands, respectively, with a wide impedance bandwidth and high gain in the second band. However, the first band has limited bandwidth, and the antenna itself has a large physical size.

The article [30] describes a dual-band, wideband composite patch antenna that utilizes a modified circular primary patch and a secondary parasitic patch element. This antenna was designed to operate in the 28/38 GHz bands and was printed on a Rogers Ro 3003 TM substrate with a dielectric constant of 3 and dimensions of $7.5 \times 8.8 \times 0.25$ mm^3. The antenna has impedance-matching bandwidths of 1.23 GHz at 28 GHz and approximately 1.06 GHz at 38 GHz. The reflection coefficient for the 28 GHz band has a minimum value of -34.5 dB, while the minimum value for the 38 GHz band is -27.3 dB. The radiation pattern has a peak gain of 6.6 dBi at 28 GHz and 5.86 dBi at 38 GHz.

In [31], a dual-band microstrip patch antenna with dimensions of 15×10 mm^2 was proposed for use in the 28/38 GHz frequency bands. The antenna utilized Rogers 5880 as its substrate material, with a thickness of 0.508 mm, a loss tangent of 0.0009, and a dielectric constant of 2.2. The antenna's gain was measured to be 7.1 dB at 28 GHz and 7.9 dB at 38 GHz, with impedance bandwidths of 1 GHz (27.6 GHz - 28.6 GHz) and 1.2 GHz (37.4 GHz - 38.6 GHz) in the respective frequency bands.

The authors of the publication [32] presented a rectangular antenna for the 60 GHz frequency band. The antenna has dimensions of 4.84 x 3.18 x 0.308 mm^3 and was fed using a quarter-wave transformer line. Resonance was achieved by loading the patch with two identical E-shaped slits. The antenna was positioned on a Rogers RT 5880 substrate with a relative permittivity of 2.2, a tangent loss ($tan\delta$) of 0.0009, and a thickness of 0.308 mm. The design offers an impedance bandwidth of 2.97 GHz (ranging from 58.67 GHz to 61.64 GHz); with a maximum return loss of 39.27 dB and a VSWR of 1.022. The design also achieved a maximum radiation efficiency of 91.7%, a maximum gain of 8.63 dBi (at 58 GHz), and a gain of 8.40 dBi at the resonance frequency.

The preceding discussion highlights that some proposed antenna designs suffer from poor gain, non-multiband functionality, or large dimensions. Although certain designs have a high gain and wide bandwidth, they are too massive for smartphone integration. Additionally, the planned 5G bands of 28 GHz, 38 GHz, and 60 GHz exhibit considerable path loss, necessitating tiny yet high-gain antennas that can cover the required frequency bands.

This study aims to balance antenna size, impedance bandwidth, and gain, achieved by developing a small but high-gain antenna with multi-band functionality and sufficient impedance bandwidth. The High-Frequency Structural Simulator (HFSS), which employs the Finite Element Method (FEM), is utilized for design, simulation, and optimization. The accuracy of the simulation results is verified using Computer Studio Technology (CST), which utilizes the Finite Integration Technique (FIT).

The remainder of the paper is structured as follows: Section II describes the proposed antenna design while Section III examines the impact of various antenna parameters on S_{11} performance. Section IV presents the simulation results for the optimized antenna's characteristics, and Section V summarizes the article's conclusions and outlines future directions.

II. The Tri-Band Antenna Design

In this work, we aim to design a rectangular antenna that is suitable for 5G smartphones and can operate in the approved frequency bands of 28 GHz, 38 GHz, and 60 GHz. Our goal is to achieve optimal multi-band functionality, high gain, and high radiation efficiency while minimizing the antenna's size. We will describe the design process leading to the final design in this section, utilizing HFSS software for design, simulation, and antenna optimization.

A. The Design Steps

Developing a millimeter-frequency microstrip antenna requires considering three critical aspects. Firstly, determining the resonant frequencies of the antenna is crucial. Secondly, selecting the dielectric substrate material used to build the

antenna and specifying its properties, such as thickness, dielectric constant, and loss tangent, is important. Fig. 1 illustrates the five major phases involved in developing the final optimized antenna design.

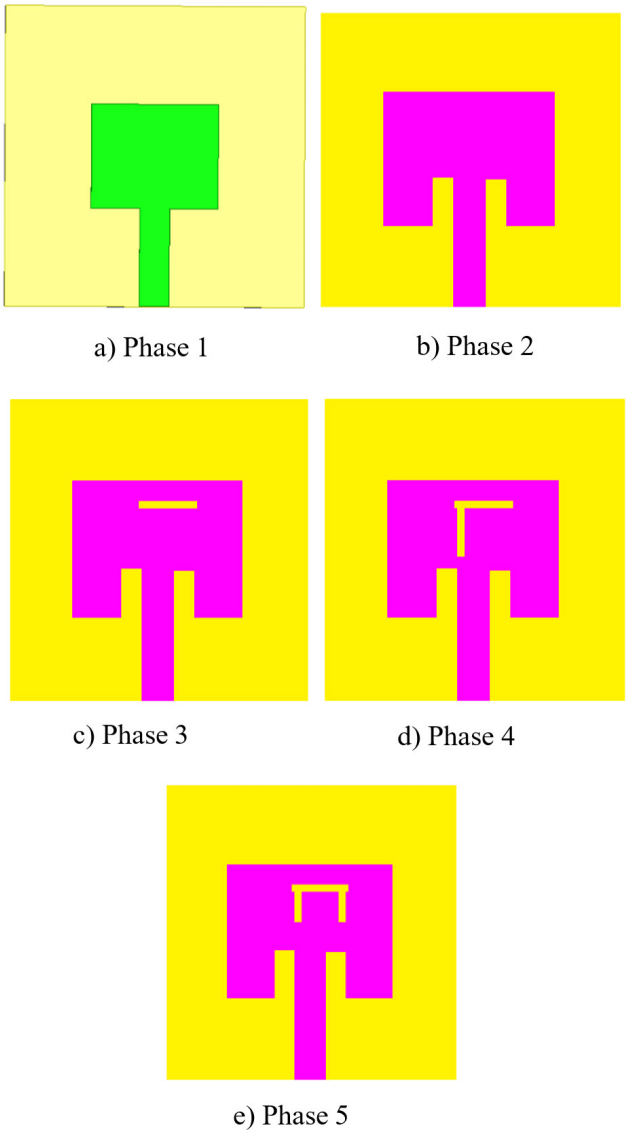

a) Phase 1 b) Phase 2

c) Phase 3 d) Phase 4

e) Phase 5

Fig. 1. The development of the proposed tri-band antenna.

Initially, the antenna design utilized the dielectric material RT/Duroid 5880, which has a dielectric constant of 2.2 and a loss tangent of 0.0009, and targeted a frequency of 28 GHz. However, the initial design, shown in Fig. 1 (a) exhibited poor return loss performance and resonated at 53 GHz. To enhance the return loss performance, the matching between the radiating patch and its feeding line was improved using the inset feed technique as seen in Fig. 1 (b). The updated design achieved resonance at 28 GHz and a return loss of approximately 36 dB, while a new frequency band around 46 GHz was observed. In the third phase, an I-shaped slot was etched horizontally on the upper side of the patch as seen in Fig. 1 (c), which slightly improved the return loss at around 42 GHz, while the resonance remained at 28 GHz with a slight decrease in the return loss value. In the fourth phase, a second I-shaped slot was etched perpendicular to the previous slot on the left side of the radiating patch as shown in Fig. 1 (d). The resonance in the second band shifted to the left, with a noticeable improvement in the value of its return loss. A third band around 63 GHz also appeared with the inclusion of the second slot. To cover the frequency ranges of 28 GHz, 38 GHz, and 60 GHz, a third I-shaped slot was etched perpendicular to the first horizontal slot, forming the symbol π as seen in Fig. 1 (e). After adding the third slot, the resonant frequency in the second band moved to around 38 GHz, while the resonant frequency in the third band moved to around 56 GHz, with a clear improvement in the return loss values in the second and third bands. It is observable that the insertion of slots on the radiating element causes only a very slight shift in resonance at 28 GHz. This unnoticeable shift could be because slots' insertions did not significantly alter the current distribution at that resonance frequency. However, the return loss value is affected by the insertion of slots.

B. The Final Optimized Design

Figure 2 depicts the final optimized tri-band antenna geometry, which consists of a rectangular patch on the top face of the dielectric substrate material and a copper sheet with a thickness of 0.035 mm on the opposite face. The substrate material's size is $8 \times 8.5 \times 0.508$ mm^3, and the patch has a π-shaped slot and is fed by a microstrip line connected through an inset feed. The optimal dimensions of the final design are summarized in Table I.

The S_{11} performance of the antenna throughout the five phases of the design process is shown in Fig. 3. The blue dashed line represents the S_{11} performance of the final optimized design, which has resonance frequencies of 27.9 GHz, 38.4 GHz, and 56 GHz, operating in three bands: 28 GHz, 38 GHz, and 60 GHz. The relative return loss levels for each band are 15.4 dB, 18 dB, and 26.4 dB, respectively. The bandwidths for each band are adequate, with the first spanning from 27.245 to 28.505 GHz, the second spanning from 37.775 to 38.855 GHz, and the third spanning from 51.725 to 63.74 GHz.

III. Parametric Analysis

To achieve the necessary frequency bands with a wide frequency range and improve impedance matching, a parametric

TABLE I.
DIMENSIONS OF THE FINAL OPTIMIZED DESIGN

Parameter	Dimension (mm)	Parameter	Dimension (mm)
Sub length (Ls)	8	Feed length (Lf)	3.6
Sub width (Ws)	8.5	Inset width (Wg)	0.395
Sub thick	0.508	Inset length (Lg)	1.002
Pat length (Lp)	4.24	Slot width (Sw)	0.2
Pat width (Wp)	3.288	Horizontal Slot length (Sl)	1.4
Pat thickness	0.035	Vertical. Slot length (Lso)	0.8
Feed width (Fw)	0.9992	π-shaped slot position (X)	1.5

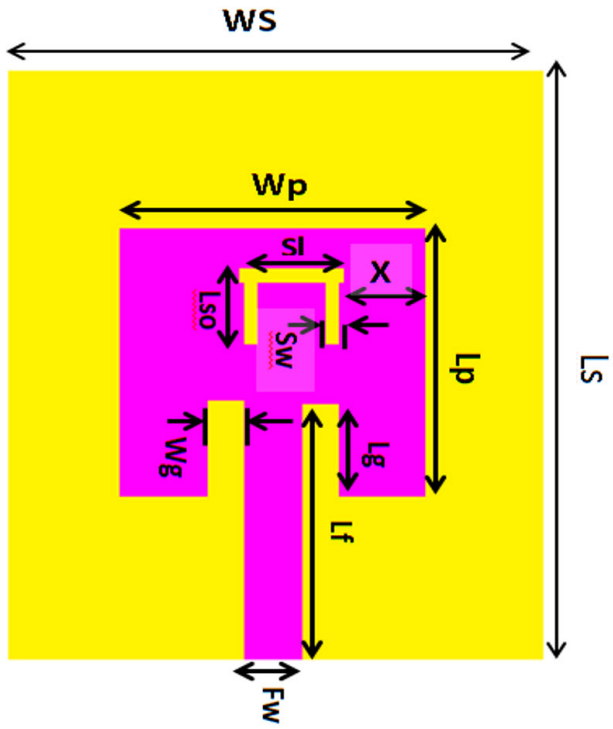

Fig. 2. The final optimized proposed tri-band antenna.

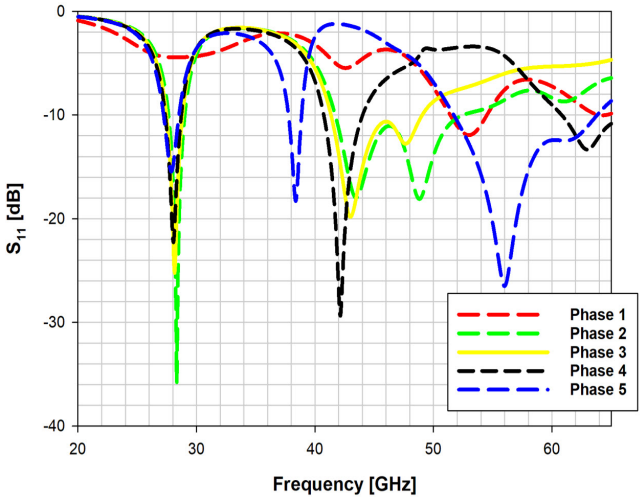

Fig. 3. The return loss performance for the design phases of the antenna.

study was conducted on some critical factors. This section investigates the effects of varying the following variables on the proposed antenna's performance: inset gap width (Wg), I-shaped slot width (Sw), slot length (Lso), microstrip feed width (Fw), and π-shaped slot location (X). By adjusting these parameters, the antenna's performance can be optimized to achieve the desired results.

A. Effects of Inset Gap Width (Wg)

Figure 4 illustrates the return loss performance for various Wg values. It can be observed that this parameter affects the return loss value without impacting the resonant frequencies. When the Wg variable is adjusted to 0.195 mm, the return loss value at 28 GHz is reduced, causing the bandwidth surrounding 28 GHz to vanish. However, the return loss levels at 38 GHz and 56 GHz are improving. When the Wg value increases to 0.395 mm, the return loss value at 28 GHz increases to around 15 dB while slightly decreasing at 38 GHz and 56 GHz to about 18 dB and 26 dB, respectively. Notably, there is a significant increase in bandwidth at 56 GHz, which is beneficial as we aim to achieve the widest bandwidths possible. To determine if the return loss values and bandwidth continue to improve, the Wg variable is further increased to 0.595 mm. However, Fig. 4 shows that while the return loss values at 28 GHz and 56 GHz increase, the return loss value at 38 GHz deteriorates, and the bandwidth at 56 GHz also shrinks. If the Wg value continues to increase, it is expected that the bandwidth at 38 GHz will vanish, and the bandwidth at 56 GHz will further contract. Therefore, the value of 0.395 mm is deemed the most suitable and ideal value for the Wg parameter.

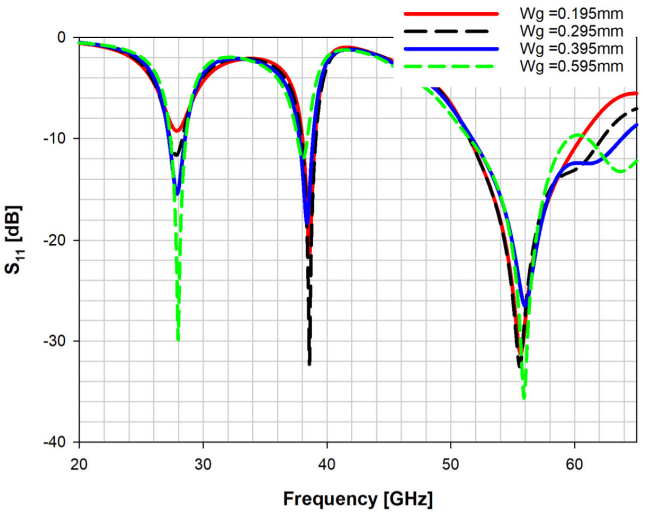

Fig. 4. Effect of inset gap width (Wg) on the S_{11} performance.

B. Effects of Slot Width (Sw)

Figure 5 illustrates the return loss performance of the proposed antenna for various I-shaped slot width values (Sw). At an Sw of 0.1 mm, the antenna covers only the 28 GHz band with a return loss value of approximately 28.5 dB and a second band around 43 GHz. Increasing Sw to 0.2 mm generates three bands, including the 28 GHz and 60 GHz bands, with a wide bandwidth spanning from 51.7 GHz to about 64 GHz. When Sw is further increased to 0.3 mm, the resonance frequency in the second band shifts to 40 GHz with a reduction in return loss value, and the resonance frequency in the third band shifts with a significant decrease in return loss value. Therefore, 0.2 mm is determined to be the optimal value for this parameter.

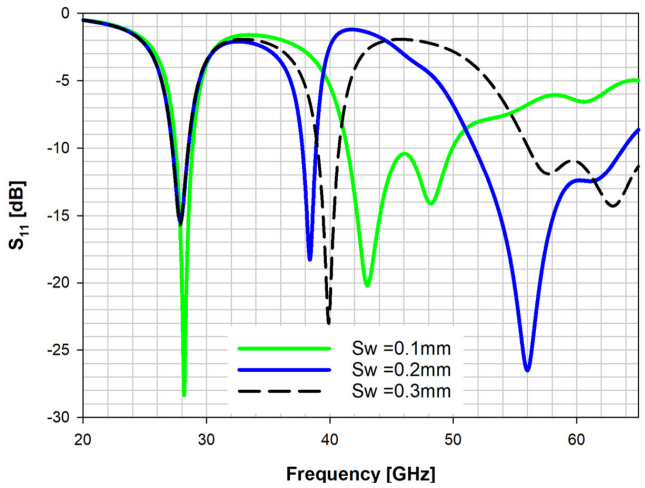

Fig. 5. Effect of the slot width (Sw) on the S_{11} performance.

C. Effects of Feeding Line Width (Fw)

The return loss curves for various feeding line width values (Fw) are shown in Fig. 6. It can be observed that the optimal value for Fw is 0.9992 mm, which yields the best performance with satisfactory return loss values for the desired frequency bands. When Fw is set to 0.5992 mm, a degradation in return loss values is observed in all three frequency bands, with the resonance shifting beyond the 38 GHz frequency and below the 28 GHz band.

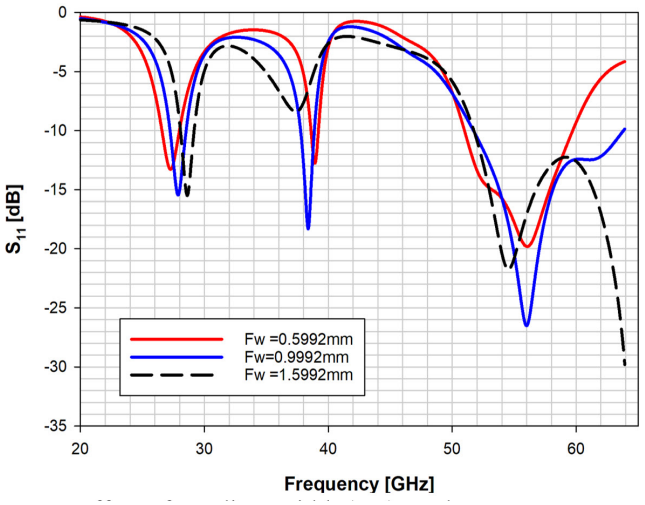

Fig. 6. Effect of the slot width (Sw) on the S_{11} performance.

Additionally, the bandwidth of the third band decreases. Increasing Fw to 1.5992 mm causes the second band at 38 GHz to disappear, and the resonance in the first band shifts beyond 28 GHz while the resonance in the third band moves below 56 GHz with a significant drop in its bandwidth. Therefore, the optimal value for the Fw parameter is determined to be 0.9992 mm, which ensures the desired frequency bands are established with acceptable return loss values.

D. Effects of slot length (Lso)

Figure 7 illustrates the S_{11} performance of the proposed design for various Lso values. It can be observed that Lso is a significant factor, and changing its value results in a noticeable difference in S_{11}'s performance. When Lso is set to 0.8 mm, the design operates in the target 28/38/60 GHz frequencies, as shown by the blue solid line curve. If the value of Lso is increased to 1 mm, the return loss at 28 GHz falls to around 13 dB, while the resonant frequency in the second band shifts to 36 GHz. In addition, the resonance in the third band changes to 53 GHz with a slight decrease in return loss value, but the bandwidth remains the same. If the value of Lso is decreased to 0.6 mm, the resonance in the first band shifts below 27 GHz, and the second band, it shifts to 40 GHz. The return loss values of the first and second bands also increase. Lowering

Lso always results in the resonance crossing 56 GHz in the third band, along with decreased return loss and bandwidth. Therefore, the optimum value for the Lso parameter to achieve the desired goals is 0.8 mm.

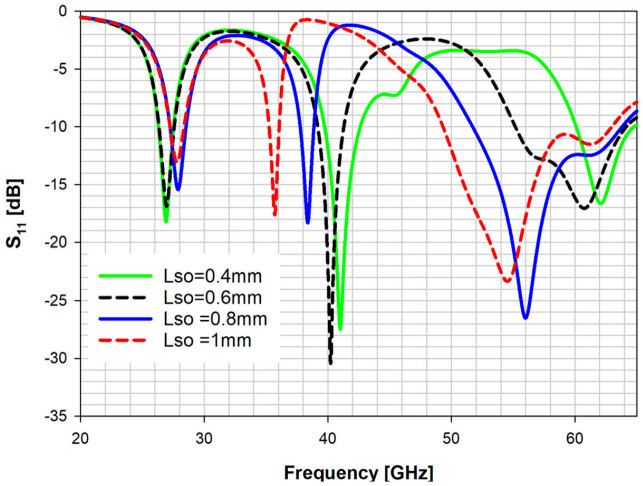

Fig. 7. Effect of slot length (Lso) on the S_{11} performance.

E. Effect of the π-shaped slot position (X)

In this section, we consider the location of the π-shaped slot with the patch's right edge (X) and examine its impact on S_{11} performance. Figure 8 shows the consequences of changing X on the proposed antenna's S_{11} performance. When X is set to 1.2 mm, the resonance occurs at 28 GHz with a 21 dB return loss. The resonance in the second band shifts to 42 GHz, although the return loss value is around 28 dB. If X is increased to 1.3 mm, the resonance frequency in the second band drops to 37 GHz, while the resonance frequencies in the first and third bands remain fixed. However, the return loss in the first band drops to around 12.5 dB. When X is set to 1.5 mm, the resonance occurs at 27.8 GHz, 38.4 GHz, and 56 GHz, establishing the three desired bands. If X is increased to 1.7 mm, the resonance in the second band shifts to 40 GHz, although the resonance in the first and third bands and the value of the third band's bandwidth remain unchanged. However, the return loss values in the first and second bands have slightly increased. Therefore, the optimum value for the X parameter to achieve the desired goals is 1.5 mm.

IV. Results and Discussion

In this section, the designed antenna's performance will be evaluated. A performance examination of the proposed antenna's reflection coefficient, 2D and 3D radiation characteristics, voltage standing wave ratio (VSWR), surface current distribution, antenna gain, and radiation efficiency will all be

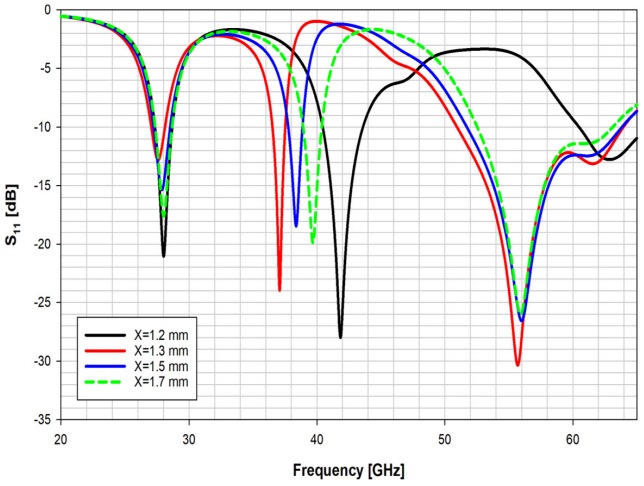

Fig. 8. Effect of the π-shaped slot position (X) on the S_{11} performance.

taken into consideration throughout the assessment. HFSS and CST, two well-known electromagnetic simulators, will be used for this evaluation. The HFSS Simulator is used to carry out the design, simulations, and optimization activities. We will simulate the optimized antenna again using the CST and compare the results from the two simulators to validate the HFSS simulation results since manufacturing and measurement capabilities are not available in our country.

A. The reflection coefficient

The antenna's reflection coefficient is the ratio of reflected RF power to the power delivered into the antenna, expressed in decibels (dB). A low return loss indicates efficient power transmission into the antenna, while a high return loss indicates significant power reflection, resulting in poor antenna performance. Therefore, optimal antenna performance requires low return loss. Antenna design, frequency of operation, and impedance matching can affect return loss and should be considered during antenna system design and evaluation.

The optimized design was simulated using both HFSS and CST software, with results presented in Fig. 9. The antenna resonates at 27.9 GHz, 38.4 GHz, and 56 GHz, with corresponding return losses of 15.4 dB, 18 dB, and 26.4 dB, respectively. The antenna also has a bandwidth of 1.26 GHz around 27.9 GHz, 1.08 GHz around 38.4 GHz, and 12.015 GHz around 56 GHz. Overall, the optimized design has good performance characteristics concerning return loss and impedance bandwidth, confirmed by simulation results from both HFSS and CST software. Generally, the simulated results show a good agreement, except for a noticeable deviation observed at 38.4 GHz in the CST curve. At 38.8 GHz, the S_{11} value did not fall below the -10 dB threshold, as shown

in Fig. 9 (where $S_{11} \approx$ -9.85). However, if a less stringent - 6 dB threshold is considered, the bandwidth at this frequency band will appear.

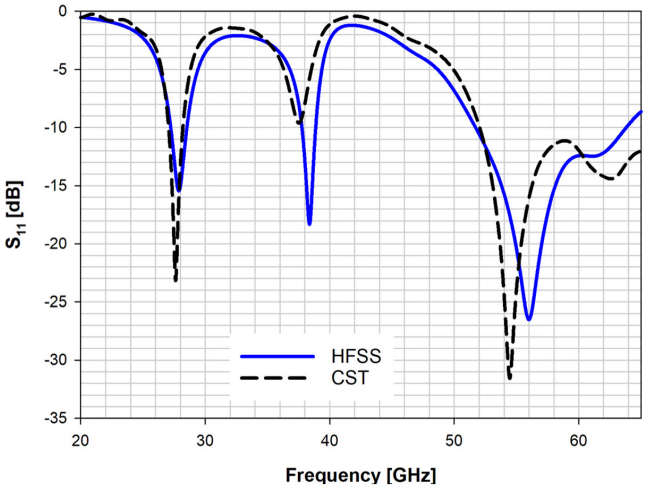

Fig. 9. Simulated S_{11} performance of the proposed antenna using HFSS and CST.

B. The Voltage Standing Wave Ratio (VSWR)

VSWR is used to measure the level of impedance mismatch between the feeding system and the antenna. As VSWR increases, so does the level of mismatch. The ideal match is achieved when VSWR has an absolute minimum value of unity. In this case, the simulation results show VSWR values of 1.405, 1.281, and 1.099 at frequencies of 27.9, 38.4, and 56 GHz, respectively, as displayed in Fig. 10 (the blue line). Additionally, the VSWR for the three operational frequencies falls between 1 and 2, indicating that the antenna and the feed line have excellent impedance matching and there are minimal reflections. HFSS and CST simulations generally agreed, except for VSWR at 38.4 GHz, which is slightly less than 2 and matched S_{11} at the same resonance frequency ($S_{11} \approx$ -9.85). Note that S_{11} = - 10 dB corresponds to VSWR $\approx$ 1.922.

C. Radiation characteristics

The gain of an antenna is an important performance factor that represents its electrical efficiency and directivity. Our antenna design exhibits a 3D gain, as shown in Fig. 11, with maximum values of 7.96 dBi, 6.82 dBi, and 7.93 dBi at the resonant frequencies, respectively. The 2D radiation patterns at the resonance frequencies for phi = 0^o and phi = 90^o, displayed in Fig. 12, show good consistency between the simulated patterns obtained from HFSS and CST. It should be noted that, as shown in Fig. 12 (a, b), the antenna radiates the highest power in the broadside direction at 27.9 GHz. Moreover, as

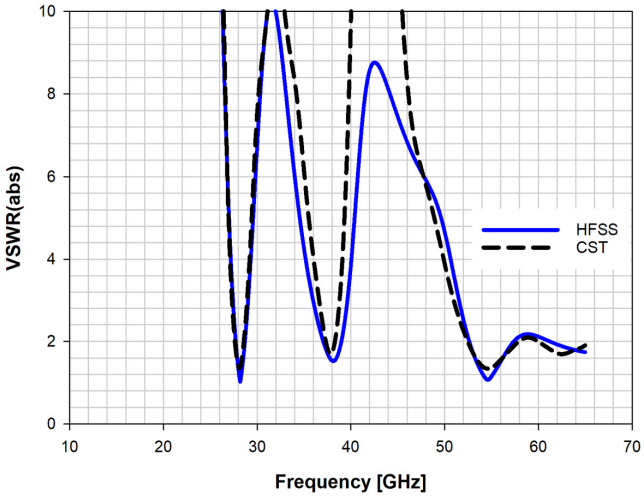

Fig. 10. Simulated VSWR of the proposed antenna using HFSS and CST.

shown in Fig. 12 (c-f), the antenna's maximum radiation level at 38.4 GHz is detected at - $41^o/41^o$, while at 56GHz, the maximum radiation occurs at -$30^o/30^o$.

Figure 13 shows the gain and efficiency of the proposed antenna as a function of operating frequencies as predicted by CST. The gain ranges from 7.54 dB to 7.6 dB in the 27.9 GHz band, 5.4 dB to 6.4 dB in the 38.4 GHz band, and 7.6 dB to 8.25 dB in the 56 GHz band. The gains calculated using CST and HFSS simulation software are very close, with maximum values of 7.96 dBi (HFSS), 7.51 dBi (CST) at 27.9 GHz, 6.82 dBi (HFSS), 6.03 dBi (CST) at 38.4 GHz, and 7.93 dBi (HFSS), 8.17 dBi (CST) at 56 GHz, respectively. Moreover, Fig. 13 illustrates the radiation efficiency of the proposed antenna, which is 88%, 84%, and 90% at 27.9 GHz, 38.4 GHz, and 56 GHz, respectively.

D. Surface Current Distribution

Surface current distribution refers to the varying flow of electric current on the surface of an antenna. It is an important characteristic that determines the radiation pattern and efficiency of the antenna. In Fig. 14, the surface current distribution of the suggested antenna is displayed at resonant frequencies of 27.9 GHz, 38.4 GHz, and 56 GHz. The figure indicates that the feed line, borders of the feed gaps, and the edges of the slots exhibit the highest current distribution. This information is significant as it provides insights into the performance of the antenna and can be used to optimize its design to achieve better efficiency and radiation characteristics.

E. Comparison with Some Published Works

Table II provides a comprehensive comparison of the proposed antenna in this paper with several recent publications.

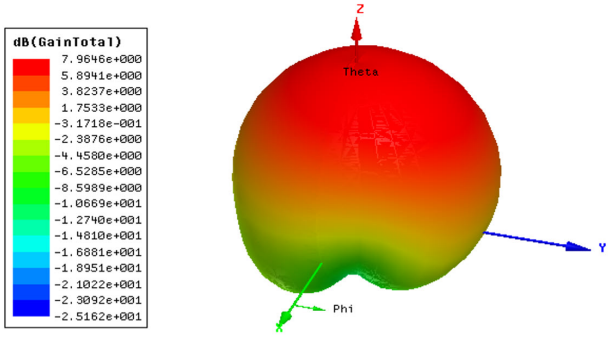

(a) at 27.9 GHz

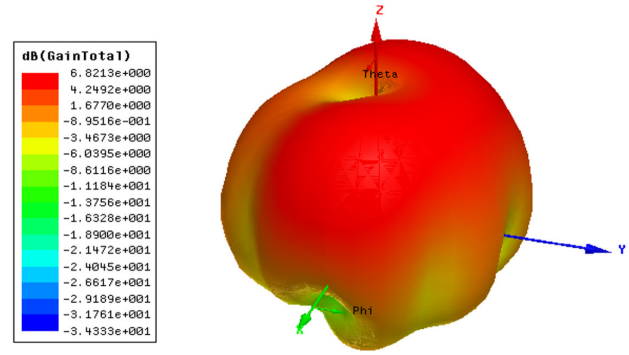

(b) at 38.4 GHz

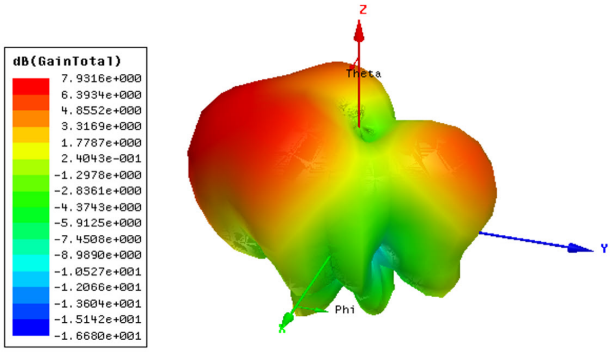

(c) at 56 GHz

Fig. 11. The 3D radiation pattern of the proposed antenna at the resonance frequencies using HFSS.

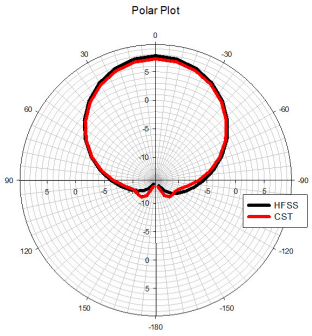

(a) 27.9 GHz (phi = 0°)

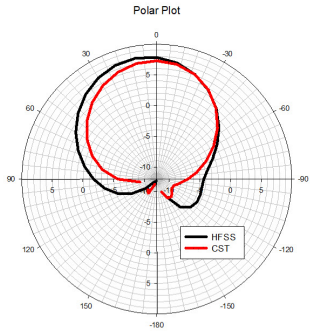

(b) 27.9 GHz (phi = 90°)

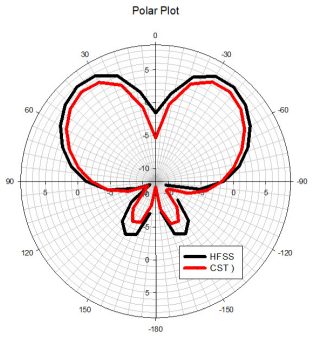

(c) 38.4 GHz (phi = 0°)

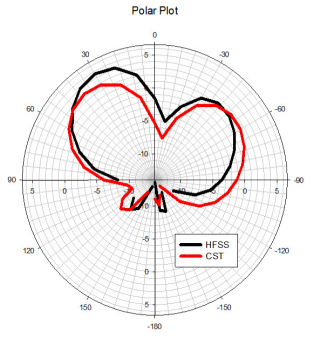

(d) 38.4 GHz (phi = 90°)

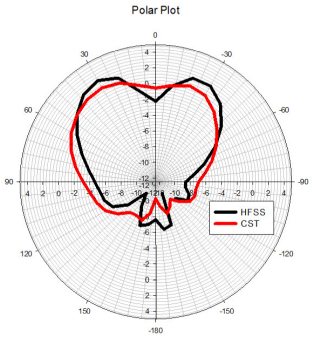

(e) 56 GHz (phi = 0°)

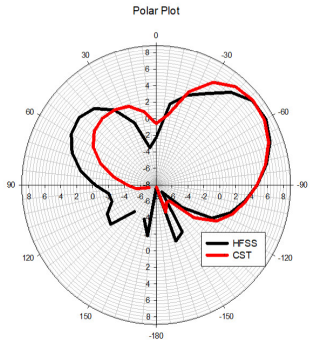

(f) 56 GHz (phi = 90°)

Fig. 12. Simulated 2D radiation patterns at the resonant frequencies, (a) at 27.9GHz (phi = 0^o), (b) at 27.9GHz (phi = 90^o), (c) at 38.4GHz (phi = 0^o), (d) at 38.4GHz (phi = 90^o), (e) at 56GHz (phi = 0^o), and (f) at 56GHz (phi = 90^o).

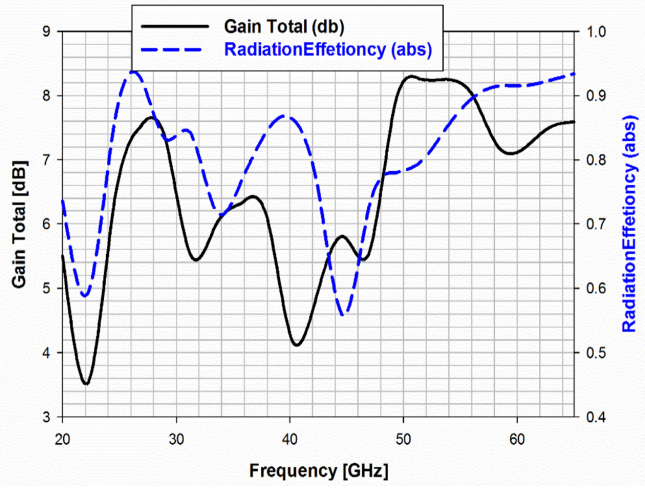

Fig. 13. The antenna gain and radiation efficiency vs operating frequencies using CST.

The comparison includes a range of performance metrics such as S_{11}, antenna dimensions, impedance bandwidth, gain, and radiation efficiency. The proposed antenna outperforms all antennas presented in references [23]- [32] concerning impedance bandwidth and exhibits superior gain compared to the antennas in [23], [25], [26], [30], and [31]. Additionally, while the proposed antenna operates in three frequency bands, the other antennas in the table are either single or dual-band, except for the antenna in [26]. However, despite the triple-band functionality of the antenna in [26], our proposed antenna demonstrates better performance in terms of both gain and impedance bandwidth.

V. Conclusion

This paper presented a low-profile tri-band antenna for 5G applications in the frequency bands of 28 GHz, 38 GHz, and 60 GHz. The antenna's matching was enhanced using an inset feed, and the radiating element was optimized by adding a π-shaped slot to improve its characteristics. The design used a Rogers RT/Duroid-5880 substrate resulting in a final antenna size of 8 x 8.5 x 0.508 mm³. The proposed antenna achieved maximum S11 values of -15.4 dB, -18 dB, and -26.4 dB at the resonant frequencies, respectively. The bandwidths achieved are 1.26 GHz, 1.08 GHz, and 12.015 GHz, respectively. In addition, the gains realized at the resonance frequencies are 7.96 dBi, 6.82 dBi, and 7.93 dBi, respectively, with high radiation efficiencies of 88%, 84%, and 90%. In addition, it is observed that the antenna radiates at the highest power in the broadside direction at 27.9 GHz, while the maximum radiation occurs at – 41/ 41 degrees and – 30/30 degrees at 38.4 GHz, and 56 GHz, respectively. The proposed design was optimized using

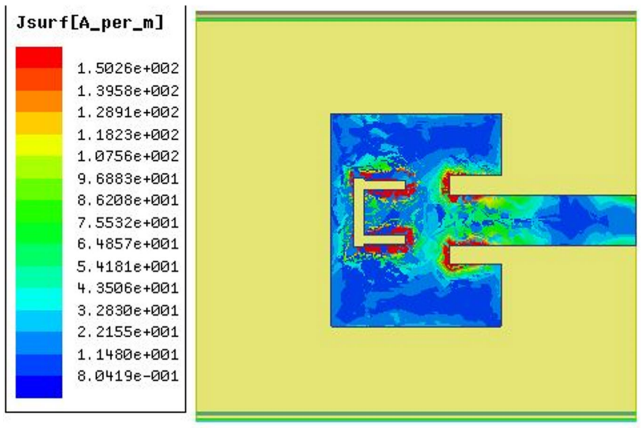

(a) at 27.9 GHz

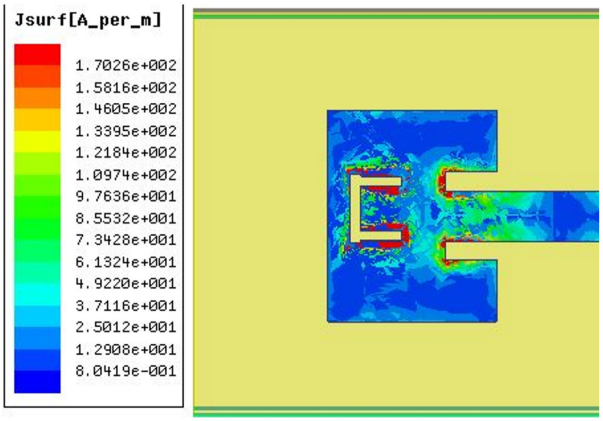

(b) at 38.4 GHz

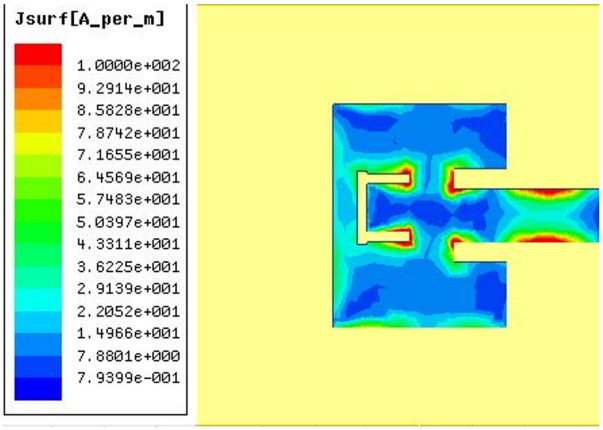

(c) at 56 GHz

Fig. 14. The surface current distribution using HFSS at (a) 27.9 GHz, (b) 38.4 GHz, and (c) 56 GHz.

TABLE II.
COMPARISON WITH SOME RECENTLY PUBLISHED LITERATURE

Ref.	Antenna Size mm^3	Frequency (GHz)	S_{11} (dB)	Gain (dBi)	BW (GHz)	Rad Efficiency %
[23]	$7 \times 7 \times 1.28$	23.52, 28,39	$\leq -43, \leq -30$	5.51, 4.55	1.16, 0.634	87, 81
[24]	$7.5 \times 27.06 \times 0.254$	28.13, 37.97	- 25.3, - 11.2	7.27, 8.46	0.231, 0.090	88.3, 86.3
[25]	$8 \times 8 \times 0.787$	27.77	- 25.45	7	1.88	74
[26]	$5.1 \times 5 \times 0.254$	28, 38, 61	-12, - 22, - 12	7.2, 7.22, 6.5	0.84, 0.37, 0.9	86, 91, 85
[27]	$20.4 \times 26.4 \times 0.508$	28,,38	- 30, -42	7.03, 7.368	0.7, 12	96, 95
[28]	$12.9 \times 14 \times 1.6$	60.06	- 24	8.62	12.11	82.2
[29]	$20 \times 16.5 \times 0.508$	25.98, 28.2	- 24.1, - 25.5	8.63, 11.26	0.55, 1.1	95.9, 95.4
[30]	$7.5 \times 8.8 \times 0.25$	28, 38	- 34.5, - 27.3	6.6, 5.86	1.23, 1.06	-
This work	$8 \times 8.5 \times 0.508$	27.9, 38.4, 56	- 15.4, - 18, - 26.4	7.96, 6.82, 7.93	1.26, 1.08, 12.015	88, 84, 90

HFSS and validated using CST, demonstrating a reasonable agreement between the simulation results. Overall, the proposed antenna offers a compact and efficient solution for 5G applications in the mentioned frequency bands. In the future, we plan to further enhance the antenna's performance. Unfortunately, due to the limited availability of fabrication and measurement facilities at our university and the ongoing civil war in our country, we were unable to fabricate and measure the antenna ourselves. Therefore, we aim to collaborate with other organizations to manufacture and measure the antenna, to validate its characteristics.

CONFLICT OF INTEREST

The authors have no conflict of relevant interest to this article.

REFERENCES

[1] E. Dahlman, G. Mildh, S. Parkvall, J. Peisa, J. Sachs, Y. Selen, and J. Skold, "5g wireless access: requirements and realization," *IEEE Communications Magazine*, vol. 52, no. 12, pp. 42–47, 2014.

[2] H. A. Diawuo and Y.-B. Jung, "Broadband proximity-coupled microstrip planar antenna array for 5g cellular applications," *IEEE Antennas and Wireless Propagation Letters*, vol. 17, no. 7, pp. 1286–1290, 2018.

[3] M. Omar, A. S. M. Mohamadariff Othman, S. Kamal, M. F. B. Ain, R. Hussin, F. Najmi, S. A. Sundi, Z. A. Ahmad, U. Ullah, and M. Faiz, "Mathematical model on the effects of conductor thickness on the center frequency at 28 ghz for the performance of microstrip patch antenna using air substrate for 5g application," *Alexandria Engineering Journal*, vol. 60, pp. 5265–5273, 2021.

[4] S. Mathew, K. Wang, Y. Azar, G. N. Wong, R. Mayzus, H. Zhao, J. K. Schulz, S. Sun, F. Gutierrez, and T. S. Rappaport, "28 ghz angle of arrival and angle of departure analysis for outdoor cellular communications using steerable beam antennas in new york city," in *In 2013 IEEE 77th Vehicular Technology Conference (VTC Spring)*, pp. 1–6.

[5] Y. Banday, G. M. Rather, and G. R. Begh, "Effect of atmospheric absorption on millimeter wave frequencies for 5g cellular networks," *IET Communications*, vol. 13, no. 3, pp. 265–270, 2019.

[6] K.-L. A. Yau, J. Qadir, C. Wu, M. A. Imran, and M. H. Ling, "Cognition-inspired 5g cellular networks: A review and the road ahead," *IEEE Access*, vol. 6, pp. 35072–35090, 2018.

[7] R. N. Mitra and D. P. Agrawal, "5g mobile technology: A survey," *ICT Express*, vol. 1, no. 3, pp. 132–137, 2015.

[8] P. Pirinen, "A brief overview of 5g research activities," in *In 1st International Conference on 5G for Ubiquitous Connectivity*, pp. 17–22, IEEE.

[9] A. N. Uwaechia and N. M. Mahyuddin, "A comprehensive survey on millimeter wave communications for fifth-generation wireless networks: Feasibility and challenges," *IEEE Access*, vol. 8, pp. 62367–62414, 2020.

[10] P. K. Gkonis, P. T. Trakadas, and D. I. Kaklamani, "A comprehensive study on simulation techniques for 5g networks: State of the art results, analysis, and future challenges," *Electronics*, vol. 9, no. 3, p. 468, 2020.

[11] L. Wei, R. Q. Hu, Y. Qian, and G. Wu, "Key elements to enable millimeter wave communications for 5g wireless systems," *IEEE Wireless Communications*, vol. 21, no. 6, pp. 136–143, 2014.

[12] Y. B. Zikria, S. W. Kim, M. K. Afzal, H. Wang, and M. H. Rehmani, "5g mobile services and scenarios: Challenges and solutions," *Sustainability*, vol. 10, no. 10, p. 3626, 2018.

[13] T. S. Rappaport, S. Sun, R. Mayzus, H. Zhao, Y. Azar, K. Wang, G. N. Wong, J. K. Schulz, and M. Samimi,

"Millimeter wave mobile communications for 5g cellular: It will work!," *IEEE Access*, vol. 1, pp. 335–349, 2013.

[14] H. Wei, Z. H. Jiang, C. Yu, D. Hou, H. Wang, C. Guo, Y. Hu, and et al, "The role of millimeter-wave technologies in 5g/6g wireless communications," *IEEE Journal of Microwaves*, vol. 1, no. 1, pp. 101–122, 2021.

[15] W. Xiong, L. Kong, F. Kong, F. Qiu, M. Xia, S. Arnon, and G. Chen, "Millimeter wave communication: A comprehensive survey," *IEEE Communications Surveys & Tutorials*, vol. 20, no. 3, pp. 1616–1653, 2018.

[16] L. C. Paul, S. C. Das, N. Sarker, M. F. Ishraque, R. Azim, and M. Z. Mahmud, "A low profile microstrip patch antenna with dgs for 5g application," in *In 2021 International Conference on Science & Contemporary Technologies (ICSCT)*, pp. 1–5, IEEE.

[17] M. Hussain, E. M. Ali, S. M. R. Jarchavi, A. Zaidi, A. I. Najam, A. A. Alotaibi, A. Althobaiti, and S. S. Ghoneim, "Design and characterization of compact broadband antenna and its mimo configuration for 28 ghz 5g applications," *Electronics*, vol. 11, no. 4, p. 523, 2022.

[18] O. Y. Saeed, A. A. Saeed, A. S. Gaid, A. M. Aoun, and A. A. Sallam, "Multiband microstrip patch antenna operating at five distinct 5g mm-wave bands," in *In 2021 International Conference of Technology, Science and Administration (ICTSA)*, pp. 1–5, IEEE.

[19] A. S. Mohammed, S. Kamal, M. B. Ain, Z. A. Ahmad, Z. Zahar, and R. Hussin, "Improving the gain performance of 2× 2 u-slot air substrate patch antenna array operated at 28 ghz wideband resonance for 5g application," in *In IOP Conference Series: Materials Science and Engineering*, vol. 917, IOP.

[20] A. S. Gaid, A. M. Alhakimi, O. Y. Sae'ed, M. S. Alasadee, and A. A. Ali, "Compact and bandwidth efficient multi-band microstrip patch antennas for 5g applications," in *In International Conference of Reliable Information and Communication Technology*, pp. 663–672, Springer.

[21] A. S. Gaid, O. A. Qaid, M. A. Ameer, F. F. Qaid, and B. S. Ahmed, "Small and bandwidth efficient multi-band microstrip patch antennas for future 5g communications," in *In International Conference of Reliable Information and Communication Technology*, pp. 653–662, Springer.

[22] A. S. Gaid, M. H. Qasem, A. A. Sallam, and E. Q. Shayea, "Dual-band rectangular microstrip patch antenna with csrr for 28/38 ghz bands applications," in *In International Conference of Reliable Information and Communication Technology*, pp. 717–727, Springer.

[23] C. L. Bamy, F. M. Mbango, D. B. O. Konditi, and P. M. Mpele, "A compact dual-band dolly-shaped antenna with parasitic elements for automotive radar and 5g applications," *Heliyon*, vol. 7, no. 4, 2021.

[24] U. Singh and R. Mishra, "A dual-band high-gain substrate integrated waveguide slot antenna for 5g applications," *Progress In Electromagnetics Research C*, vol. 119, pp. 191–200, 2022.

[25] D. G. Patanvariya and A. Chatterjee, "A compact bow-tie shapedwide-band microstrip patch antenna for future 5g communication networks," *Radioengineering*, vol. 30, no. 1, pp. 40–47, 2021.

[26] M. Ur-Rehman, M. Adekanye, and H. T. Chattha, "Triband millimeter-wave antenna for body-centric networks," *Nano Communication Networks*, vol. 18, pp. 72–81, 2018.

[27] F. Alnemr, M. F. Ahmed, and A. A. Shaalan, "A compact 28/38 ghz mimo circularly polarized antenna for 5 g applications," *Journal of Infrared, Millimeter, and Terahertz Waves*, vol. 42, pp. 338–355, 2021.

[28] M. M. Khan, K. Islam, M. N. A. Shovon, M. Baz, and M. Masud, "Design of a novel 60 ghz millimeter wave q-slot antenna for body-centric communications," *International Journal of Antennas and Propagation*, vol. 2021, pp. 1–12, 2021.

[29] M. Nahas, "A super high gain l-slotted microstrip patch antenna for 5g mobile systems operating at 26 and 28 ghz," *Engineering, Technology & Applied Science Research*, vol. 12, pp. 8053–8057, 2022.

[30] A. E. Farahat and K. F. Hussein, "Dual-band (28/38 ghz) wideband mimo antenna for 5g mobile applications," *IEEE Access*, vol. 10, pp. 32213–32223, 2022.

[31] K. Raheel, A. Altaf, A. Waheed, S. H. Kiani, D. A. Sehrai, F. Tubbal, and R. Raad, "E-shaped h-slotted dual band mm-wave antenna for 5g technology," *Electronics*, vol. 10, no. 9, p. 1019, 2021.

[32] Z. N. Alhaj, A. Saif, and A. S. Gaid, "A rectangular microstrip patch antenna loaded with two identical e-shaped slits for 60 ghz band applications," in *In 2022 2nd International Conference on Emerging Smart Technologies and Applications (eSmarTA)*, pp. 1–6, IEEE.